

# Development of an analytical model to estimate the churning losses in high-speed axial piston pumps

Qun CHAO (✉)<sup>a,b</sup>, Jianfeng TAO<sup>a</sup>, Chengliang LIU<sup>a</sup>, Zhengliang LI<sup>c</sup>

<sup>a</sup> State Key Laboratory of Mechanical System and Vibration, School of Mechanical Engineering, Shanghai Jiao Tong University, Shanghai 200240, China

<sup>b</sup> State Key Laboratory of Fluid Power and Mechatronic Systems, School of Mechanical Engineering, Zhejiang University, Hangzhou 310027, China

<sup>c</sup> Liyuan Hydraulic (Suzhou) Co., Ltd., Suzhou 215131, China

✉ Corresponding author. E-mail: chaoqun@sjtu.edu.cn (Qun CHAO)

© Higher Education Press 2022

**ABSTRACT** The axial piston pumps in aerospace applications are often characterized by high-speed rotation to achieve great power density. However, their internal rotating parts are fully immersed in the casing oil during operation, leading to considerable churning losses (more than 10% of total power losses) at high rotational speeds. The churning losses deserve much attention at the design stage of high-speed axial piston pumps, but accurate analytical models are not available to estimate the drag torque associated with the churning losses. In this paper, we derive the analytical expressions of the drag torque acting on the key rotating parts immersed in oil, including the cylinder block and the multiple pistons in a circular array. The calculated drag torque agrees well with the experimental data over a wide range of rotational speeds from 1500 to 12000 r/min. The presented analytical model provides practical guidelines for reducing the churning losses in high-speed axial piston pumps or motors.

**KEYWORDS** axial piston pump, rotating parts, high rotational speed, churning losses, drag torque

## 1 Introduction

Hydraulic systems are widely used in the fields of construction, agriculture, robotics, automobile, and aerospace due to their high power density. Axial piston pumps are known as the “heart” of hydraulic systems, given that they supply pressurized fluid to other components downstream in the system, such as valve, cylinder, and motor. The maximum rotational speed of axial piston pumps has been increasing during the last decades to meet the market demands for smaller size and higher power density, especially in aerospace applications [1]. At present, the speed limitation of axial piston pumps can reach up to more than 10000 r/min in aerospace applications [2,3], which is about 10 times higher than that in construction applications.

As typical rotating machinery, axial piston pumps contain a group of rotating parts in an enclosed fluid-filled casing to accomplish the basic task of fluid suction and discharge. The rotating parts generate considerable

power losses at high rotational speeds, leading to low pump efficiency and high temperature rise of the casing fluid. Figure 1 shows the power losses in three commercial axial piston motors that have similar rotating parts to axial piston pumps. The power losses in each axial piston motor increase significantly with the rotational speed. It is reasonable to believe that axial piston pumps also have significant power losses at high rotational speeds. Therefore, accurate prediction of power losses is crucial for axial piston pumps, especially at the early design stage without available tests.

According to Refs. [4–6], the power losses in an axial piston pump mainly come from three sources: volumetric, mechanical, and churning losses. The volumetric losses result from the gap leakage in lubricating interfaces and the fluid compressibility. The mechanical losses arise from the friction at the tribological contacts between movable parts. Many theoretical and experimental studies have been devoted to load-dependent volumetric and mechanical losses [7–9]. Unlike the former two load-dependent power losses, the churning losses are no-load dependent power losses that are associated with the drag

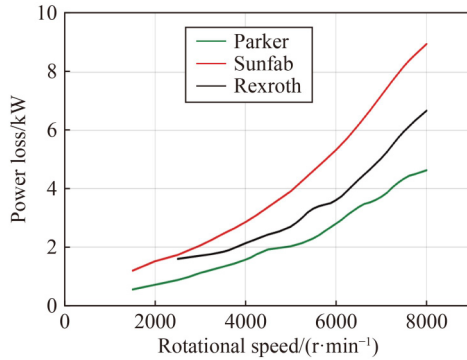


**Fig. 1** Power losses in three commercial axial piston motors at variable rotational speeds.

torques generated by the rotating parts stirring the surrounding hydraulic fluid.

The rotating parts in the oil-filled casing generate flow around multiple circular cylinders, including shaft, cylinder block, and pistons. During the last few decades, considerable effort has been made to study the flow around circular cylinders numerically and experimentally [10,11]. For instance, Singh et al. [12] numerically examined the flow interference between two circular cylinders at different orientations and observed that the downstream cylinder had much lower drag coefficient than the upstream cylinder in the case of tandem arrangement. Yang et al. [13] experimentally studied the flow configuration of three equilateral-triangular circular cylinders and found unique features of flow interference in comparison with two cylinders. Yin et al. [14] numerically investigated the flow patterns around nine cylinders at low Reynolds number and discovered that the flow patterns strongly depended on the gap ratio between two cylinders.

The churning losses are an important contributor to the pump power losses, especially at high rotational speed, low operating pressure, and small displacement [4,5,15]. Thus, they have attracted growing interest from academic and industrial communities. For example, Olsson [4] measured the churning losses in an actual axial piston pump and estimated that the churning losses accounted for 15%–20% of the total power losses. Xu et al. [16] and Zhang et al. [17] established a preliminary analytical model for the churning losses and carried out computational fluid dynamics and semi-physical simulations to evaluate the effects of rotational speed on the churning losses. In particular, Zhang et al. [17] built a specific test rig to acquire the individual contribution of cylinder block and pistons to the total churning losses by comparing the drag torques between wet and dry casings. Similarly, Jing et al. [18] and Hasko et al. [19] measured the churning losses of rotating parts in a commercial axial piston pump through the differences in input torque between oil-filled and empty casings. Zecchi et al. [6] and Zhang et al. [20] considered the churning losses in the

total power losses when predicting the casing fluid temperature in an axial piston pump. Moslått et al. [21] included the churning losses of rotating parts when deducing the torque losses in variable displacement axial piston motors. The researchers also found that the churning losses account for a large portion of power losses in other types of high-speed hydraulic pumps, such as 2D piston pumps [22,23] and radial ball piston pumps [24].

Practical methods for reducing the churning losses have been proposed in terms of rotating parts/casing structure and hydraulic fluid usage in the axial piston pump/motor. Parker Hannifin Corporation invented a “power boost insert” embedded in the motor casing for minimal fluid friction and oil compression, reducing the power losses by up to 5 kW (about 13%) at high rotational speeds [25]. Theissen et al. [5] and Zhang et al. [26] confirmed the effectiveness of the “power boost insert” in churning loss reduction through simulation and experimental results. Li et al. [27] and Theissen et al. [5] discovered that a nano-coated cylinder block and a low-viscosity hydraulic fluid could generate low churning loss in axial piston pumps by numerical and experimental analyses. Furthermore, Rahmfeld et al. [15] claimed that the dry motor casing could save a noticeable energy up to 5% in the driveline by experimentally comparing the power losses between wet and dry motor casings at various rotational speeds.

In summary, the researchers have paid increasing attention to the churning losses in axial piston pumps in recent years. Previous studies focused on methods for churning loss measurement and reduction. Several studies have also presented analytical models for the drag torques acting on the rotating parts associated with the churning losses in axial piston machines. Particularly, the prior work [17] compared the calculated and measured drag torques acting on the rotating parts (cylinder block and pistons) in an axial piston pump. However, the comparison results revealed a large discrepancy between the model and measurements, especially at high rotational speeds. Therefore, this work aims to extend the prior work [17] by improving the prediction accuracy of churning losses in high-speed axial piston pumps. A new analytical model for churning losses will be established and validated with the existing experimental data.

## 2 Machine description

An axial piston pump is a type of positive displacement machines, which can convert rotating mechanical energy into hydraulic power by changing the displacement chamber volumes periodically. Figure 2 schematically shows a typical swash plate-type axial piston pump. The rotating parts of the pump are comprised of a shaft, a cylinder block, multiple pistons, and slippers. The pistons are connected to the slippers via ball-and-socket joints

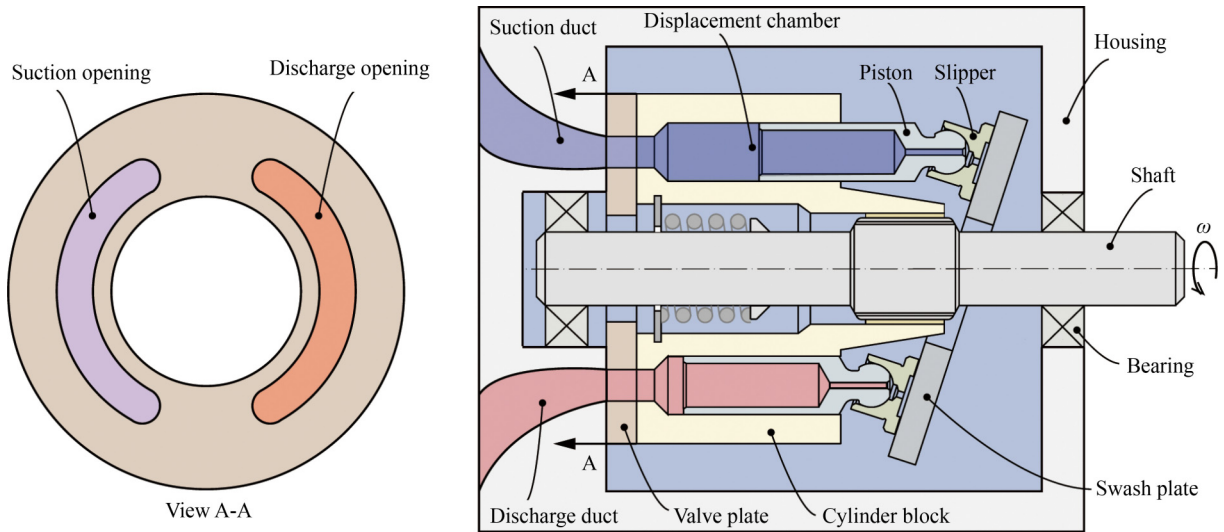


**Fig. 2** Schematic of an axial piston pump. Reprinted with permission from Ref. [3] from Springer Nature (Copyright 2021).

and are evenly accommodated in the cylinder block bores. The rotating parts are supported by two bearings at the shaft ends and held against the valve plate by a compressed spring. Once the shaft drives the rotating parts, the slippers slide on the inclined swash plate and force the pistons to reciprocate in the cylinder block bores. The periodical change of the displacement chamber volumes completes the task of continuous fluid suction and discharge through the cylinder block ports and two openings in the valve plate.

In addition to the above internal flow, the rotating parts also create an external flow surrounding them because they are fully immersed in a hydraulic fluid. The hydraulic fluid that fills up the enclosed pump housing is responsible for lubricating friction pairs [28] and dissipating the generated heat during the pump operation. However, the immersed rotating parts generate additional power losses (also called churning losses) due to the interaction between the rotating parts and the external fluid. Actually, the external flow surrounding the rotating parts can be regarded as a special flow around multiple circular cylinders. The friction drag and pressure drag acting on these circular cylinders consume a portion of input torque of the pump. In the next section, we will derive the drag torques acting on the cylinder block and pistons in an axial piston pump. The shaft contributes little to the total churning losses compared with the cylinder block and pistons; hence, its drag torque is neglected in this work.

### 3 Analytical model

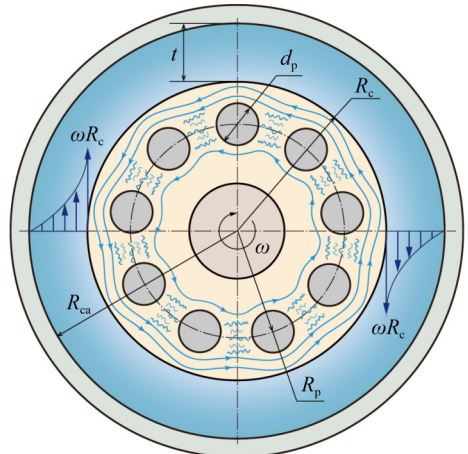
The parameters influencing the churning losses of the rotating parts are as follows: (a) the multi-cylinder geometry characterized by piston number  $N$ , piston diameter  $d_p$ , piston length  $L_p$ , piston pitch circle radius  $R_p$ ,

casing internal radius  $R_{ca}$ , cylinder block external radius  $R_c$ , and cylinder block length  $L_c$ ; (b) the fluid properties, i.e., density  $\rho$  and kinematic viscosity  $\nu$ ; and (c) the rotational speed  $\omega$ . **Figure 3** illustrates the layout of the rotating parts immersed in oil, as well as their main dimensions.

#### 3.1 Churning losses of cylinder block

The inside wall of the casing is simplified into a perfect cylindrical surface concentric with the cylinder block wall [6,16]. In this case, the fluid flow enclosed by the cylinder block and the casing can be considered a common annular flow between two concentric cylinders. The drag torque ( $T_c$ ) acting on the rotating cylinder block can be expressed as

$$T_c = \frac{1}{2} C_{dc} \pi \rho \omega^2 R_c^4 L_c, \quad (1)$$



(Casing) (Oil) (Cylinder block) (Shaft) (Piston)

**Fig. 3** Schematic of the rotating parts immersed in oil.

where  $C_{dc}$  is the drag coefficient of the cylinder block that depends on the Reynolds number and the annular dimensions. On the basis of the work by Bilgen and Boulos [29], the drag coefficient is written as

$$C_{dc} = \begin{cases} \lambda_1 Re_c^{-\lambda_2} \left( \frac{R_{ca} - R_c}{R_c} \right)^{\lambda_3} & \text{for } 500 < Re_c < 1 \times 10^4, \\ \lambda_4 Re_c^{-\lambda_5} \left( \frac{R_{ca} - R_c}{R_c} \right)^{\lambda_6} & \text{for } Re_c > 1 \times 10^4, \end{cases} \quad (2)$$

where  $Re_c$  is the Reynolds number associated with the cylinder block rotation, which is defined as

$$Re_c = \frac{\omega R_c (R_{ca} - R_c)}{v}. \quad (3)$$

The constant coefficients  $\lambda_1, \lambda_2, \dots, \lambda_6$  in Eq. (2) are determined from experimental data in principle. For simplicity, the coefficients  $\lambda_1$  and  $\lambda_4$  are set to 1.03 and 0.065, respectively, and the coefficients  $\lambda_3$  and  $\lambda_6$  are both set to 0.3 in accordance with the work by Bilgen and Boulos [29]. In this case, the drag coefficient of the rotating cylinder block can be further expressed as

$$C_{dc} = \begin{cases} 1.03 Re_c^{-\lambda_2} \left( \frac{R_{ca} - R_c}{R_c} \right)^{0.3} & \text{for } 500 < Re_c < 1 \times 10^4, \\ 0.065 Re_c^{-\lambda_5} \left( \frac{R_{ca} - R_c}{R_c} \right)^{0.3} & \text{for } Re_c > 1 \times 10^4. \end{cases} \quad (4)$$

Given  $m$  operating points at rotational speeds of  $\omega_1, \omega_2, \dots, \omega_m$ , we can calculate the drag torque acting on the cylinder block by using Eqs. (3) and (4). The constant coefficients in Eq. (4) are determined by minimizing the mean squared error between calculated and measured drag torques.

$$\{\lambda_2, \lambda_5\} = \arg \min \sum_1^m \left( \frac{T_{cm} - T'_{cm}}{T'_{cm}} \right)^2, \quad (5)$$

where  $T_{cm}$  and  $T'_{cm}$  are the calculated and measured drag torques at rotational speed of  $\omega_m$ , respectively. Note that  $\lambda_2$  and  $\lambda_5$  need to satisfy the equation  $\lambda_2 = \lambda_5 + 0.3$  to ensure a continuous drag coefficient at the critical Reynolds number of  $1 \times 10^4$ .

### 3.2 Churning losses of multiple pistons

The churning losses of the rotating parts account for a great proportion of the total power in the axial piston pump at a small displacement [4,5,24]. Therefore, this study focuses on the churning losses at zero displacement, in which individual pistons no longer reciprocate in the cylinder block bores and they have an identical overhang length. For modelling simplicity, we assume that the slippers have the same diameter as the pistons and regard them as an integrated body.

The pistons are nested in the cylinder block at equal

angular intervals and can be regarded as a group of rotating circular cylinders. The calculated drag torque acting on all pistons ( $T_p$ ) is expressed as

$$T_p = \frac{N}{2} C_{dp} \rho \omega^2 R_p^3 L_p d_p, \quad (6)$$

where  $C_{dp}$  is the drag coefficient of a single piston.

Typically, the drag coefficient for a circular cylinder is a function of the Reynolds number  $f(Re_p)$ , and its curve against the Reynolds number is available from many fluid mechanics textbooks [30]. However, the drag coefficient of a single piston is less than that of a circular cylinder at the same Reynolds number due to the shielding effect between adjacent pistons [6]. In this case, we modify the drag coefficient of the piston by considering the shielding effects.

$$C_{dp} = \left( \frac{2\pi R_p - Nd_p}{Nd_p} \right)^{f(Re_p)} C_D = k_p^{f(Re_p)} C_D, \quad (7)$$

where  $k_p = (2\pi R_p - Nd_p)/(Nd_p)$  is the dimensionless relative gap between two adjacent pistons, and  $f(Re_p)$  is its power; and  $C_D$  is the Reynolds number-related drag coefficient of a single circular cylinder. Both  $f(Re_p)$  and  $C_D$  are related to the nominal Reynolds number  $Re_p = \omega R_p d_p / v$  of a single piston.

Substituting the measured drag torque  $T'_p$  and Eq. (7) into Eq. (6) yields

$$f(Re_p) = \frac{\ln(2T'_p) - \ln(NC_D \rho \omega^2 R_p^3 L_p d_p)}{\ln k_p}. \quad (8)$$

We can obtain the approximate function  $f(Re_p)$  by fitting the experimental curve of  $f(Re_p)$  versus the nominal Reynolds number  $Re_p$  at various rotational speeds.

---

## 4 Experimental procedure

**Figure 4** shows an overview of the specific churning test rig and the simplified rotating parts of an axial piston pump. The test rig mainly consisted of a test pump, a torque/speed sensor, and an electric motor. The test pump was a swash plate-type axial piston pump with nine pistons. Its main specifications were as follows: theoretical maximum and minimum volumetric displacements of 7.25 and 0.6 cm<sup>3</sup>/r, respectively, rated rotational speed of 10000 r/min, and rated outlet pressure of 28 MPa. The rotating parts of the test pump included a shaft, a cylinder block, and nine pistons. **Table 1** details the geometric characteristics of the rotating parts. The cylinder block and shaft were fabricated into an integrated body, and the multiple pistons were fixed to the cylinder block with threaded connection. The bearing supported the rotating parts that were fully submerged in hydraulic oil. The standard density and kinematic viscosity of the hydraulic oil were 850 kg/m<sup>3</sup> and 32 mm<sup>2</sup>/s, respectively, at 40 °C. The electric motor drove the rotating parts up to a

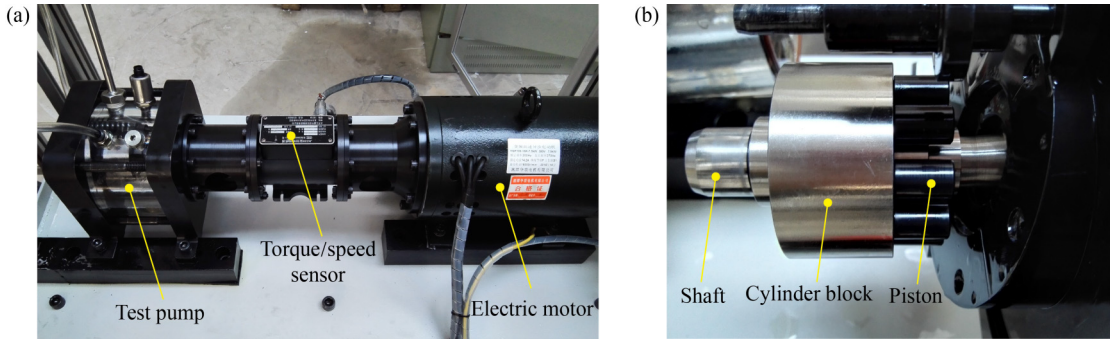


**Fig. 4** Photos of (a) specific churning test rig and (b) simplified rotating parts.

**Table 1** Geometric dimensions of the rotating parts [17]

Geometric dimension	Value
Cylinder block external radius, $R_c/\text{mm}$	28
Cylinder block length, $L_c/\text{mm}$	32.5
Piston pitch circle radius, $R_p/\text{mm}$	20
Casing internal radius, $R_{ca}/\text{mm}$	42.5
Piston number, $N$	9
Piston diameter, $d_p/\text{mm}$	10
Piston length, $L_p/\text{mm}$	11.45

maximum of 12000 r/min by a coupling, and the rotational speed was controlled by a frequency converter. A torque/speed sensor was used to simultaneously measure the rotational speed and input torque of the rotating parts. The pressure and temperature of the casing oil were monitored using a pressure sensor and a temperature sensor, respectively.

The total no-load power losses consisted of the churning losses of the rotating parts and the friction losses of the shaft bearings and seals. The basic idea to isolate the net churning losses was subtracting the power losses with empty casing from that with oil-filled casing at the same rotational speed. Specifically, the input torque was measured in the case of empty casing and oil-filled casing at rotational speeds from 1500 to 12000 r/min. Note that, strictly speaking, the input torque with empty casing included the windage losses of the rotating parts in addition to the friction losses of the shaft bearings and seals. Fortunately, the windage losses are generally negligible compared with the churning losses. Additionally, the friction losses of the shaft bearings and seals under no-load conditions were almost constant regardless of whether the casing was empty or full of oil [31]. Therefore, in this work, the net drag torque of the rotating parts was approximately equal to the torque difference between oil-filled casing and empty casing.

The drag torque acting on the cylinder block and the multiple pistons needed to be measured separately. First, the multiple pistons were connected to the cylinder block to obtain the total net torque acting on the rotating parts. Then, all pistons were disconnected from the cylinder

block to obtain the net torque acting on the cylinder block, given that the drag torque acting on the shaft was much lower than that acting on the cylinder block. Finally, the net drag torque acting on the multiple pistons could be obtained by subtracting the net drag torque acting on the cylinder block from the total net torque acting on the rotating parts with multiple pistons.

## 5 Results and discussion

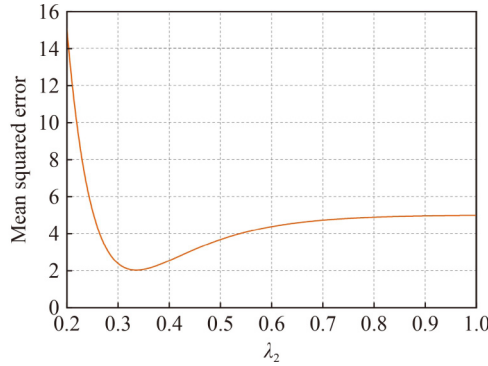
### 5.1 Churning losses of cylinder block

The mean squared error of the drag torque acting on the cylinder block achieves its minimum value at  $\lambda_2 = 0.336$ , as shown in Fig. 5. Substituting  $\lambda_2 = 0.336$  into Eq. (4) yields the final expression for the drag coefficient of the rotating cylinder block.

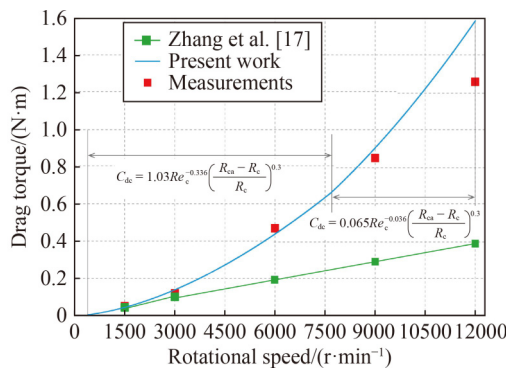
$$C_{dc} = \begin{cases} 1.03Re_c^{-0.336} \left( \frac{R_{ca} - R_c}{R_c} \right)^{0.3} & \text{for } 500 < Re_c < 1 \times 10^4, \\ 0.065Re_c^{-0.036} \left( \frac{R_{ca} - R_c}{R_c} \right)^{0.3} & \text{for } Re_c > 1 \times 10^4. \end{cases} \quad (9)$$

Figure 6 compares the drag torque acting on the cylinder block between the experimental data and the calculation results of this work and previous work by Zhang et al. [17]. Equations (1) and (9) have captured the basic physics of churning losses of the cylinder block with some deviations near the high rotational speed range. The relative value of the deviation ranges from  $-13\%$  to  $15\%$  at 1500–9000 r/min, and it increases to  $26\%$  at 12000 r/min. The drag torque is overestimated at high rotational speeds for two possible reasons. First, cavitation occurs near the rotating cylinder block due to high-velocity shear [17], and the entrained bubbles reduce the friction drag. Second, the churning losses generate considerable heat that reduces the fluid viscosity.

By contrast, the previous model significantly underestimates the drag torque acting on the cylinder block, especially at high rotational speeds. The significant underestimation of the drag torque results from the



**Fig. 5** Mean squared error of the drag torque acting on the cylinder block as a function of coefficient  $\lambda_2$ .



**Fig. 6** Drag torque acting on the cylinder block—Comparisons between different analytical models and the experimental measurements in Ref. [17].

assumption of a constant velocity gradient for the fluid around the rotating cylinder block [17]. That is, the fluid velocity is assumed to decrease linearly from the cylinder block surface to the casing inner wall. As a result, the calculated drag torque is proportional to the rotational speed  $\omega$ . In fact, the fluid velocity gradient is no longer constant when the flow situation occurs between two concentric cylinders rather than two parallel plates. The drag torque is proportional to  $\omega^{1.664}$  for  $500 < Re_c < 1 \times 10^4$  and to  $\omega^{1.964}$  for  $Re_c > 1 \times 10^4$  in accordance with Eqs. (1), (3), and (9).

Equation (9) shows that the drag coefficient of the cylinder block decreases with the Reynolds number at low and moderate Reynolds numbers but remains relatively constant at high Reynolds numbers. This means that the fluid viscosity has little influence on the drag torque of the cylinder block at high rotational speeds. In addition to the Reynolds number, the gap height between the cylinder block and the casing,  $t = R_{ca} - R_c$ , is another critical factor in determining the drag coefficient. Figure 7 shows how the drag coefficient varies with the rotational speed at different gap heights, in which the 14.5 mm is the actual gap height between the cylinder block and the casing in the test rig. We notice that the drag coefficient at each gap height always experiences a

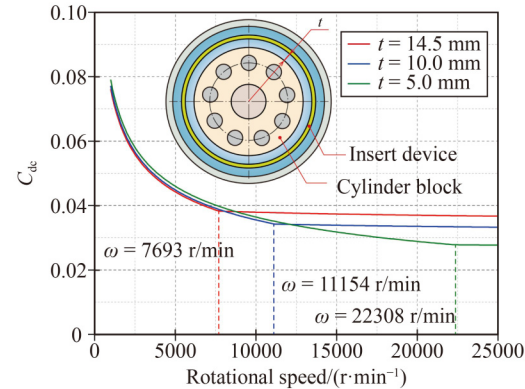


**Fig. 7** Radial gap effects on the drag coefficient of the cylinder block.

rapid decrease with increasing rotational speed and then becomes steady as the rotational speed exceeds a critical value.

The comparison of the drag coefficient at different gap heights shows that a smaller gap height generates a lower drag coefficient at high rotational speeds. For example, the drag coefficient declines by 9% and 15% at the rotational speed of 15000 r/min when the gap height becomes smaller from 14.5 to 10.0 and 5.0 mm, respectively. This finding well explains the mechanism of churning loss reduction by the insert device in high-speed axial piston pumps/motors [25,26]. Specifically, the insert device is installed between the cylinder block and the casing, acting as a temporary casing and thus reducing the actual gap height. On the other hand, a smaller gap height slightly increases the drag coefficient at low rotational speeds. For instance, the drag coefficient rises by 1% and 4% at the rotational speed of 5000 r/min as the initial gap height of 14.5 mm reduces to 10.0 and 5.0 mm, respectively. This observation agrees with the experimental results in Ref. [26], in which the drag torque acting on the cylinder block slightly increases at smaller gap heights under low-speed conditions.

We can use Eqs. (3) and (9) to explain the opposite effects of the insert device on the drag coefficient in different speed ranges. The drag coefficient in Eq. (9) can be further expressed as a function of the gap height by replacing the Reynolds number  $Re_c$  with Eq. (3).

$$C_{dc} = \begin{cases} \frac{1.03}{R_c^{0.636} t^{0.036}} \left( \frac{\nu}{\omega} \right)^{0.336} & \text{for } 500 < Re_c < 1 \times 10^4, \\ \frac{0.065 t^{0.264}}{R_c^{0.336}} \left( \frac{\nu}{\omega} \right)^{0.036} & \text{for } Re_c > 1 \times 10^4. \end{cases} \quad (10)$$

Equation (10) indicates that smaller gap heights increase the drag coefficient in a low Reynolds number range (i.e., low rotational speeds) but decrease the drag coefficient in a high Reynolds number range (i.e., high rotational speeds). Therefore, the insert device should be used in high-speed axial piston pumps/motors rather than low-speed ones in terms of churning losses.

The gears and bearings partially immersed in an oil sump also suffer churning losses. Similar experimental and theoretical studies on them have emphasized the impacts of fluid volume on the churning losses [32,33]. Expressing the drag torque acting on the cylinder block as a function of the casing fluid volume is practical in engineering applications because the product manuals usually offer the information about the casing fluid volume in an actual pump/motor. For simplification purposes, we assume that the casing fluid only exists between the cylinder block and the casing when deriving the new expression from Eq. (9). Letting  $k_r = (R_{ca} - R_c)/R_c$  or  $R_{ca} = (1 + k_r)R_c$ , the volume ratio  $\zeta$  between the casing fluid and the cylinder block is given by

$$\zeta = \frac{V_{oil}}{V_c} = \frac{\pi(R_{ca}^2 - R_c^2)L_c}{\pi R_c^2 L_c} = 2k_r + k_r^2, \quad (11)$$

where  $k_r$  is the dimensionless relative gap between the pump casing and the cylinder block,  $V_{oil}$  is the casing fluid volume, and  $V_c$  is the cylinder block volume that is assumed to be a perfect solid circular cylinder.

The constant  $k_r$  can be expressed as a function of  $\zeta$  by solving Eq. (11),

$$k_r = \frac{-2 \pm \sqrt{4 + 4\zeta}}{2} = \pm \sqrt{1 + \zeta} - 1. \quad (12)$$

When the negative root is discarded and the Maclaurin series is used, Eq. (12) can be rewritten as

$$k_r = \sqrt{1 + \zeta} - 1 = \frac{1}{2}\zeta - \frac{1}{8}\zeta^2 + R(\zeta), \quad (13)$$

where  $R(\zeta)$  is the remainder term of the Maclaurin series. The higher-order terms of  $\zeta$  in Eq. (13) can be neglected because  $\zeta$  is much less than unity for an actual axial piston pump/motor. Hence, Eq. (13) can be approximately expressed as  $k_r = \zeta/2$ .

Substituting  $k_r = \zeta/2$  into Eq. (9) yields the relationship between the drag coefficient and the casing fluid volume.

$$C_{dc} = \begin{cases} 0.84Re_c^{-0.336} \left( \frac{V_{oil}}{V_c} \right)^{0.3} & \text{for } 500 < Re_c < 1 \times 10^4, \\ 0.053Re_c^{-0.036} \left( \frac{V_{oil}}{V_c} \right)^{0.3} & \text{for } Re_c > 1 \times 10^4. \end{cases} \quad (14)$$

The volume ratio  $\zeta$  reflects the degree of compactness of the rotating parts in an axial piston pump/motor. A lower volume ratio means more compact rotating parts enclosed by the pump casing. Comparison of Eqs. (9) and (14) shows that the gap height and the volume ratio have equivalent effects on the drag torque, i.e., compact rotating parts are recommended for high-speed axial piston pumps/motors from the viewpoint of reducing churning losses.

## 5.2 Churning losses of multiple pistons

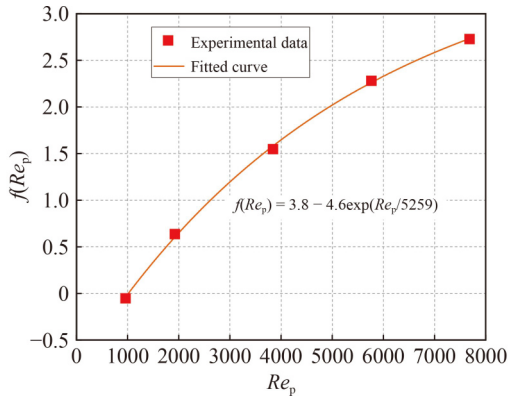
The power term  $f(Re_p)$  of the dimensionless piston gap  $k_p$

is the key point to calculate the drag coefficient of the multiple pistons, as shown in Eq. (7). Figure 8 presents the fitted curve of  $f(Re_p)$  as a function of the nominal Reynolds number  $Re_p$ , in which the value of adjusted  $R^2$ -square is 0.999. The power term  $f(Re_p)$  in Eq. (7) is replaced with the fitting function in Figure 8, and the final expression for the drag coefficient of the multiple pistons is

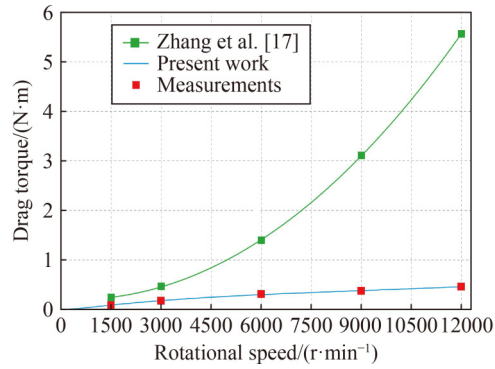
$$C_{dp} = C_D k_p^{3.8-4.6\exp(-Re_p/5259)} = C_D \left( \frac{2\pi R_p - Nd_p}{Nd_p} \right)^{3.8-4.6\exp(-Re_p/5259)}. \quad (15)$$

Figure 9 compares the measured drag torque acting on the multiple pistons with the prediction results of this work and previous work by Zhang et al. [17]. The comparison results indicate that the calculated drag torques in this work are in good match with the measurements at all operating points with a relative value of deviation less than 3%. By contrast, the previous work significantly overestimates the drag torque, especially at high rotational speeds. The large discrepancy between different calculated drag torques lies in whether the shielding effect between adjacent pistons is considered in the calculation of the drag coefficient of individual pistons. The term “shielding effect” refers to the phenomenon in which the special circular array of the multiple pistons allows each piston to shield the downstream one in the rotation direction, thus reducing the piston drag coefficient [5,6]. The previous work neglected the shielding effect and regarded each piston as an independent circular cylinder, leading to an overestimation of the piston drag coefficient. On the contrary, this work considers the shielding effect by introducing a reduction factor into the drag coefficient of a single circular cylinder, as shown in Eq. (15).

The shielding effect strongly depends on the Reynolds number and the relative gap between two adjacent pistons. Figure 10 shows how the relative gap influences the shielding effect over a wide range of Reynolds numbers, in which the shielding effect is represented by the drag coefficient rate  $C_{dp}/C_D$ . At low Reynolds numbers, the shielding effect has a negligible impact on the piston drag coefficient, and  $C_{dp}$  approximately equals  $C_D$ . With the increase in the Reynolds number, the piston drag coefficient first falls sharply and then becomes steady gradually. The onset of boundary layer separation and cavitation on the piston surface is a possible reason for the almost unchanged piston drag coefficient at extremely high Reynolds numbers. The growth trend of the piston drag coefficient implies that the shielding effect of the multiple pistons almost disappears in the laminar flow regime but apparently occurs in the turbulent flow regime. This favorable trend prevents dramatic increases in the piston drag coefficient and associated drag torque at high rotational speeds, as shown in Fig. 9.



**Fig. 8** Fitting curve of  $f(Re_p)$  versus the nominal Reynolds number.



**Fig. 9** Drag torque acting on the pistons—Comparisons between different analytical models and the experimental measurements in Ref. [17].

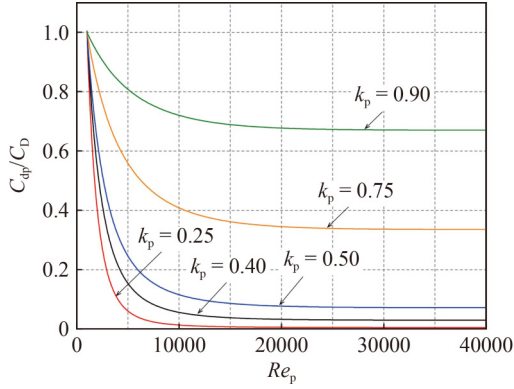


**Fig. 10** Shielding effects on the reduction in piston drag coefficient.

For an axial piston pump/motor, the empirical value of the relative gap between two adjacent pistons ranges from 0.20 to 0.50, as shown in Table 2. We can enhance the shielding effect by reducing the relative gap between two adjacent pistons, as shown in Fig. 10. Given the Reynolds number of 10000 for example, the drag coefficient rate declines by 0.043 as the relative gap decreases from 0.40 (baseline value) to 0.25; on the contrary, it rises by 0.060

**Table 2** Statistical results of  $k_p$  for a series of commercial axial piston pumps

Volumetric displacement/(mL·r <sup>-1</sup> )	N	R <sub>p</sub> /mm	d <sub>p</sub> /mm	k <sub>p</sub>
28	9	32.2	15.0	0.50
45	9	34.5	18.0	0.34
60	9	34.5	20.0	0.21
80	9	39.5	20.0	0.38
105	9	48.0	23.0	0.46
125	9	51.0	24.5	0.45
140	9	51.0	25.0	0.42
180	9	54.3	28.0	0.35
230	9	58.0	32.0	0.27
280	9	65.4	32.5	0.40

as the relative gap increases from 0.40 to 0.50. Therefore, at moderate and high Reynolds numbers, the drag coefficient reduction benefits more from smaller relative gaps because of the enhanced shielding effect. However, the drag coefficient drops more and more slowly with decreasing relative gap. For instance, the steady drag coefficient rate drops by 0.26 and 0.067 when the relative gap decreases from 0.75 to 0.50 and from 0.50 to 0.25, respectively.

Figure 10 also suggests that a combination of high Reynolds numbers and small relative gaps generates a low piston drag coefficient. The expressions  $Re_p = \omega R_p d_p / v$  and  $k_p = (2\pi R_p - Nd_p) / (Nd_p)$  indicate that the geometric parameters influencing the Reynolds number and the relative gap include the piston number, diameter, and pitch circle radius. The piston drag coefficient increases with decreasing piston number due to a larger relative gap and the consequent weaker shielding effect. As a result, a pump/motor with fewer pistons may even suffer higher churning losses in spite of the reduced pistons [5]. In addition, a smaller piston diameter leads to a higher piston drag coefficient due to decreased Reynolds number and increased relative gap. Consequently, a smaller size of the pistons may lead to higher churning losses. Enekes [34] also reported this finding after comparing the simulated churning losses between three groups of pistons with the same piston number but different piston diameters. In practice, we can minimize the churning losses by reducing the relative gap, such as increasing the piston number and diameter or decreasing the piston pitch circle radius.

### 5.3 Total churning losses of cylinder block and multiple pistons

Figure 11 further compares the total drag torque acting on the cylinder block and pistons between the predicted and experimental results. The relative value of the deviation ranges from 4.8% to 18.9% at the measured operating

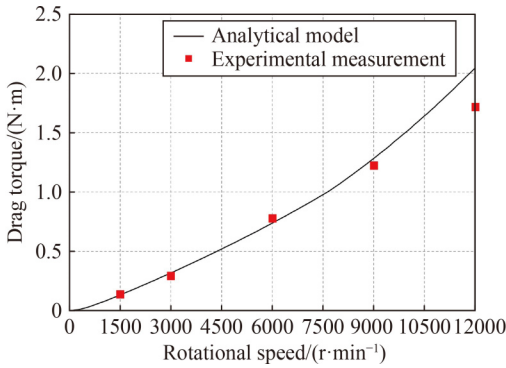


**Fig. 11** Comparison of the total drag torque acting on the cylinder block and pistons between the presented analytical model and experimental measurements in Ref. [17].

points, which demonstrates a good qualitative and quantitative agreement between the theoretical predictions and the experimental measurements. The relative error of the analytical model achieves its maximum of 18.9% at the rotational speed of 12000 r/min, while it is always less than 10% at other rotational speeds. Like the drag torque acting on the cylinder block, the overestimated total drag torque at high rotational speeds may result from the cavitation occurrence and declined viscosity.

## 6 Conclusions

This paper presents an accurate analytical model to estimate the drag torque associated with the churning losses of the rotating parts (cylinder block and multiple pistons) in an axial piston pump. The accuracy and reliability of the analytical model have been validated by the experimental measurements from a specific test rig. The following conclusions can be drawn from the analytical and experimental results:

(1) The drag coefficient of the cylinder block depends on the Reynolds number and the relative gap between the cylinder block and the pump casing. The drag torque acting on the cylinder block is proportional to  $\omega^{1.664}$  for  $500 < Re_c < 1 \times 10^4$  and to  $\omega^{1.964}$  for  $Re_c > 1 \times 10^4$ . By contrast, previous studies considered that drag torque increased linearly with rotational speed due to the assumption of a constant velocity gradient between cylinder block and casing, which would significantly underestimate the drag torque acting on the cylinder block, especially at high rotational speeds.

(2) The shielding effect between adjacent pistons helps reduce the drag coefficient of each piston. Previous studies significantly overestimated the drag torque of multiple pistons because they failed to consider the shielding effect and directly regarded the high drag coefficient of a single circular cylinder as the actual piston drag coefficient. The piston drag coefficient decreases with the increasing Reynolds number and the

decreasing relative gap. For example, the piston drag coefficient can drop by more than 10 times when the rotational speed increases from 1500 to 12000 r/min and by 75% when the relative gap between adjacent pistons decreases from 0.75 to 0.5.

(3) We can lower the churning losses of the rotating parts in high-speed axial piston pumps/motors by reducing the drag coefficient of the rotating parts. Specifically, an embedded insert device can reduce the churning losses at high rotational speeds by introducing a smaller gap height between the cylinder block and the pump casing. The smaller gap height essentially reduces the volume ratio between the casing fluid and the cylinder block. On the other hand, the insert device can slightly increase the churning losses at low rotational speeds because of boundary layer transition. Similarly, a lower piston drag coefficient can be obtained by reducing the relative gap between two adjacent pistons through considering, for example, more pistons, a smaller piston pitch circle radius, and a larger piston diameter.

(4) In addition to the geometric parameters of the rotating parts, the oil property is another important factor in determining the churning losses in axial piston pumps. A low kinematic viscosity of oil means a high Reynolds number and thus brings down the drag coefficient. The density of oil influences the churning losses from the two aspects of fluid kinetic energy and Reynolds number. A low oil density reduces the fluid kinetic energy and hence partially brings down the churning losses. At the same time, it reduces the Reynolds number and thus partially increases the drag coefficient.

The limitation of this work is that the proposed analytical models for churning losses have only been validated using the existing experimental data from an axial piston pump. Overcoming this limitation requires more physical experiments or numerical simulations with different sizes of rotating parts of the axial piston pump and motor in future work.

## Nomenclature

$C_{dc}$	Drag coefficient of the cylinder block
$C_{dp}$	Drag coefficient of a single piston
$C_D$	Reynolds number-related drag coefficient of a single circular cylinder
$d_p$	Piston diameter
$f(Re_p)$	A function of the Reynolds number
$k_p$	Dimensionless relative gap between two adjacent pistons
$k_r$	Dimensionless relative gap between the pump casing and the cylinder block
$L_c$	Cylinder block length
$L_p$	Piston length
$m$	Number of operating points

$N$	Piston number
$R_c$	Cylinder block external radius
$R_{ca}$	Casing internal radius
$R_p$	Piston pitch circle radius
$Re_c$	Reynolds number associated with the cylinder block rotation
$Re_p$	Nominal Reynolds number of a single piston
$R(\zeta)$	Remainder term of the Maclaurin series
$t$	Gap height between the cylinder block and the casing
$T_c$	Drag torque acting on the rotating cylinder block
$T_{cm}$	Calculated drag torque acting on the cylinder block at rotational speed of $\omega_m$
$T'_{cm}$	Measured drag torque acting on the cylinder block at rotational speed of $\omega_m$
$T_p$	Calculated drag torque acting on all pistons
$T'_p$	Measured drag torque acting on all pistons
$V_c$	Cylinder block volume
$V_{oil}$	Casing fluid volume
$\zeta$	Volume ratio between the casing fluid and the cylinder block
$\lambda_i$ ( $i = 1, 2, \dots, 6$ )	Constant coefficients determined from experimental data in principle
$\nu$	Kinematic viscosity
$\rho$	Fluid density
$\omega$	Rotational speed

**Acknowledgements** This study was supported by the National Key R&D Program of China (Grant No. 2021YFB2011902), the National Natural Science Foundation of China (Grant No. 52005323), the National Postdoctoral Program for Innovative Talents (Grant No. BX20200210), and the China Postdoctoral Science Foundation (Grant No. 2019M660086).

## References

- Chao Q, Zhang J H, Xu B, Huang H P, Pan M. A review of high-speed electro-hydrostatic actuator pumps in aerospace applications: challenges and solutions. *Journal of Mechanical Design*, 2019, 141(5): 050801
- Chao Q, Zhang J H, Xu B, Wang Q N, Lyu F, Li K. Integrated slipper retainer mechanism to eliminate slipper wear in high-speed axial piston pumps. *Frontiers of Mechanical Engineering*, 2022, 17(1): 1
- Chao Q, Tao J F, Lei J B, Wei X L, Liu C L, Wang Y H, Meng L H. Fast scaling approach based on cavitation conditions to estimate the speed limitation for axial piston pump design. *Frontiers of Mechanical Engineering*, 2021, 16(1): 176–185
- Olsson H. Power losses in an axial piston pump used in industrial hydrostatic transmissions. In: Proceedings of the 8th Scandinavian International Conference on Fluid Power. Tampere, 2003
- Theissen H, Gels S, Murrenhoff H. Reducing energy losses in hydraulic pumps. In: Proceedings of the 8th International Conference on Fluid Power Transmission and Control. Hangzhou, 2013, 77–81
- Zecchi M, Mehdizadeh A, Ivantysynova M. A novel approach to predict the steady state temperature in ports and case of swash plate type axial piston machines. In: Proceedings of the 13th Scandinavian International Conference on Fluid Power. Linköping, 2013, 177–187
- Xu B, Hu M, Zhang J H, Su Q. Characteristics of volumetric losses and efficiency of axial piston pump with respect to displacement conditions. *Journal of Zhejiang University-SCIENCE A*, 2016, 17(3): 186–201
- Gao M D, Huang H H, Li X Y, Liu Z F. A novel method to quickly acquire the energy efficiency for piston pumps. *Journal of Dynamic Systems, Measurement, and Control*, 2016, 138(10): 101004
- Tang H S, Ren Y, Xiang J W. Power loss characteristics analysis of slipper pair in axial piston pump considering thermohydrodynamic deformation. *Lubrication Science*, 2019, 31(8): 381–403
- Zdravkovich M M. The effects of interference between circular cylinders in cross flow. *Journal of Fluids and Structures*, 1987, 1(2): 239–261
- Hishikar P, Dhiman S K, Tiwari A K, Gaba V K. Analysis of flow characteristics of two circular cylinders in cross-flow with varying Reynolds number: a review. *Journal of Thermal Analysis and Calorimetry*, 2022, 147(10): 5549–5574
- Singh S V, Mitra P, Kumar P. A study of flow interference and heat transfer between two-cylinders at different orientations. *Journal of Ocean Engineering and Science*, 2021, 6(3): 248–256
- Yang Z J, Wang X K, Si J H, Li Y L. Flow around three circular cylinders in equilateral-triangular arrangement. *Ocean Engineering*, 2020, 215: 107838
- Yin J J, Jia T, Gao D, Xiao F. Numerical investigation of the patterns of the flow past nine cylinders at low Reynolds number. *AIP Advances*, 2020, 10(8): 085107
- Rahmfeld R, Marsch S, Göllner W, Lang T, Dopichay T, Untch J. Efficiency potential of dry case operation for bent-axis motors. In: Proceedings of the 8th International Fluid Power Conference. Dresden, 2012, 2: 73–86
- Xu B, Zhang J H, Li Y, Chao Q. Modeling and analysis of the churning losses characteristics of swash plate axial piston pump. In: Proceedings of the 2015 International Conference on Fluid Power and Mechatronics (FPM). Harbin: IEEE, 2015, 22–26
- Zhang J H, Li Y, Xu B, Pan M, Lv F. Experimental study on the influence of the rotating cylinder block and pistons on churning losses in axial piston pumps. *Energies*, 2017, 10(5): 662
- Jing C B, Zhou J J, Zhou J C. Experimental study of churning losses in swash plate axial piston pump. *Journal of Beijing Institute of Technology*, 2019, 28(3): 529–535
- Hasko D, Shang L Z, Noppe E, Lefrançois E. Virtual assessment and experimental validation of power loss contributions in swash plate type axial piston pumps. *Energies*, 2019, 12(16): 3096
- Zhang J H, Li Y, Xu B, Chen X, Pan M. Churning losses analysis on the thermal-hydraulic model of a high-speed electro-hydrostatic actuator pump. *International Journal of Heat and Mass Transfer*, 2018, 127: 1023–1030
- Moslått G A, Hansen M R, Karlsen N S. A model for torque losses

- in variable displacement axial piston motors. *Modeling, Identification and Control*, 2018, 39(2): 107–114
- 22. Huang Y, Ruan J, Zhang C C, Ding C, Li S. Research on the mechanical efficiency of high-speed 2D piston pumps. *Processes*, 2020, 8(7): 853
  - 23. Huang Y, Ding C, Wang H Y, Ruan J. Numerical and experimental study on the churning losses of 2D high-speed piston pumps. *Engineering Applications of Computational Fluid Mechanics*, 2020, 14(1): 764–777
  - 24. Bohach G. A study and optimization of a radial ball piston pump for high-speed applications. Thesis for the Master's Degree. Minneapolis: University of Minnesota, 2021
  - 25. Parker Hannifin. Hydraulic Saw Motor: Series F11/F12 Fixed Displacement. 2018
  - 26. Zhang J H, Li Y, Xu B, Pan M, Chao Q. Experimental study of an insert and its influence on churning losses in a high-speed electro-hydrostatic actuator pump of an aircraft. *Chinese Journal of Aeronautics*, 2019, 32(8): 2028–2036
  - 27. Li Y, Xu B, Zhang J H, Chen X. Experimental study on churning losses reduction for axial piston pumps. In: Proceedings of the 11th International Fluid Power Conference. Aachen, 2018, 272–280
  - 28. Hooke C J, Li K Y. The lubrication of overclamped slippers in axial piston pumps—centrally loaded behaviour. *Proceedings of the Institution of Mechanical Engineers, Part C: Journal of Mechanical Engineering Science*, 1988, 202(4): 287–293
  - 29. Bilgen E, Boulos R. Functional dependence of torque coefficient of coaxial cylinders on gap width and Reynolds numbers. *Journal of Fluids Engineering*, 1973, 95(1): 122–126
  - 30. Gerhart A L, Hochstein J I, Gerhart P M. Munson, Young and Okiishi's Fundamentals of Fluid Mechanics. 9th ed. Singapore: John Wiley & Sons, 2021
  - 31. Chen S W, Matsumoto S. Influence of relative position of gears and casing wall shape of gear box on churning loss under splash lubrication condition—some new ideas. *Tribology Transactions*, 2016, 59(6): 993–1004
  - 32. Changenet C, Velex P. Housing influence on churning losses in geared transmissions. *Journal of Mechanical Design*, 2008, 130(6): 062603
  - 33. Quiban R, Changenet C, Marchesse Y, Ville F. Experimental investigations about the power loss transition between churning and windage for spur gears. *Journal of Tribology*, 2021, 143(2): 024501
  - 34. Enekes C P. Measures to increase the efficiency of axial piston machines. Dissertation for the Doctoral Degree. Aachen: RWTH Aachen University, 2012 (in German)